Miner Deposita
DOI 10.1007/s00126-016-0637-0

LETTER

Re-Os pyrite geochronology of Zn-Pb mineralization in the giant Caixiashan deposit, NW China

Dengfeng Li[1,2,3] · Huayong Chen[1] · Pete Hollings[3] · Li Zhang[1] · Mei Mi[1] · Jie Li[4] · Jing Fang[1,2] · Chengming Wang[1,2] · Wanjian Lu[1,2]

Received: 21 July 2015 / Accepted: 8 January 2016

Abstract The newly discovered Caixiashan Irish-type Zn-Pb deposit (~131 Mt at 3.95 % Zn + Pb), located in the Eastern Tianshan of Xinjiang, is one of the largest Zn-Pb deposits in NW China. Massive colloform/framboidal textured syn-sedimentary pyrite yielded a Re-Os isochron age of 1019 ± 70 Ma (MSWD = 3.5), which is interpreted to be the depositional age of the Kawabulake group that hosts the ore. The age of the main mineralization stage is constrained by two types of pyrite: the layered pyrite coexists with recrystallized calcite and dolomite and is locally replaced by sphalerite, whereas the euhedral pyrite occurs with galena that crosscuts the massive sphalerite. The layered pyrite yielded a Re-Os age of 859 ± 79 Ma (MSWD = 6.7; initial $^{187}Os/^{188}Os$ ratio $[I_{Os}] = 0.19 \pm 0.25$) and the euhedral pyrite 837 ± 39 Ma (MSWD = 6.5; $[I_{Os}] = 0.16 \pm 0.09$), which are interpreted to be the Zn and Pb mineralization ages, respectively. The low radiogenic initial Os values of the Zn-Pb mineralization suggest interaction between a hydrothermal fluid and a mafic or ultramafic source rock with a mantle Os signature with some contamination with Mesoproterozoic Kawabulake group. Based on our new Re-Os ages, we conclude that the giant Caixiashan Zn-Pb deposit formed in the early Neoproterozoic and it represents a newly identified mineralization epoch in the Eastern Tianshan of the Central Asia Orogenic Belt.

Keywords Pyrite Re-Os · Irish-type Pb-Zn deposit · Caixiashan · Eastern Tianshan

Editorial handling: K. Kelley and G. Beaudoin

✉ Huayong Chen
huayongchen@gig.ac.cn

[1] Key Laboratory of Mineralogy and Metallogeny, Guangzhou Institute of Geochemistry, Chinese Academy of Sciences, P.O. Box 1131, Tianhe District, Guangzhou 510640, Guangdong, China

[2] Graduate University of Chinese Academy of Sciences, Beijing 100049, China

[3] Department of Geology, Lakehead University, 955 Oliver Road, Thunder Bay, ON P7B 5E1, Canada

[4] State Key Laboratory of Isotope Geochemistry, Guangzhou Institute of Geochemistry, Chinese Academy of Sciences, Guangzhou 510640, China

Introduction

The Caixiashan Zn-Pb deposit in the Eastern Tianshan area, Xinjiang, NW China, is a newly discovered giant Zn-Pb deposit with current reserves of 131 Mt at 3.95 % Zn + Pb (Cao et al. 2013). Although some research on the deposit has been conducted since its discovery in 2002, reliable metallogenic ages for the Caixiashan deposit have not been reported. To date, a number of geological models have been proposed. These include a magmatic hydrothermal origin related to Late Carboniferous magmatism (Cao et al. 2013) and a syn-sedimentary origin associated with the formation of the Precambrian Kawabulake group (Peng et al. 2008). Resolving the ages of the host rock and ore bodies will shed light on the factors controlling the Zn-Pb mineralization in the Central Tianshan Terrane.

The application of the Re-Os geochronometer to sulphide minerals, not only molybdenite but also pyrite, chalcopyrite and asenopyrite, has significantly advanced the understanding of mineralizing processes, as this method allows for the direct dating of ore-forming minerals (Stein et al. 1998; Stein et al. 2000; Morelli et al. 2004; Selby et al. 2009; Lawley and Selby

Published online: 23 January 2016

2012; Lawley et al. 2013). Accurate dating of mineralization has been a major problem in low-temperature Pb-Zn deposits (Leach et al. 2010). The majority of attempts have utilised Rb-Sr dating of sphalerite or paleomagnetic techniques, but the accuracy of both techniques has recently been disputed by comparison with reliable results based on Re-Os geochronology (Selby et al. 2005; Hnatyshin et al. 2015; David L. Leach, personal communication, 2015). Consequently, Re-Os dating of sulphides, especially pyrite, is the preferred choice for dating Zn-Pb mineralization.

Here, we present Re-Os data for three episodes of pyrite mineralization in the Caixiashan deposit, allowing us to determine the depositional age of the host rocks as well as the age of subsequent mineralization. Our Re-Os data provide evidence for a new Neoproterozoic metallogenic event in the Eastern Tianshan of the Central Asian Orogenic Belt.

Geological setting

The Eastern Tianshan is located between the Central Asian Orogenic Belt (CAOB) and the Tarim basin (Fig. 1a), and can be subdivided into the Central Tianshan terrane, the Aqishan-Yamansu arc/back-arc, the Kanggur-Huangshan shear zone and the Dananhu-Tousuquan island arc with each terrane separated by a series of E–trending faults, i.e., the Aqikekuduke, Yamansu and Kanggur faults (Fig. 1b). This collage formed as a result of the subduction and collision of the Junggar (north) and the Tarim (south) plates from the Ordovician to the Carboniferous (Allen and Natal'in 1995; Pirajno et al. 2008).

The Central Tianshan terrane is located on the southern margin of Eastern Tianshan and structurally bound by the Aqikekuduke fault in the north, the Tuokexun-Gangou fault in the southwest and the Xingxingxia fault in the southeast (Fig. 1b). The Mesoproterozoic Kawabulake group is in fault contact with Carboniferous volcanic rocks of the Aqishan-Yamansu back-arc and conformably underlain by the Mesoproterozoic carbonate rocks, dolomite and quartz schist of the Xingxingxia group. The Kawabulake group is comprised mainly of sedimentary rocks but the Xinjiang Geological Survey (1999) has recognised several mafic tuff outcrops within the group. The Kawabulake group hosts a number of economic Zn-Pb deposits including Caixiashan, Hongyuan, Jiyuan, Shaquanzi and Hongxingshan (Fig. 1b). A metamorphosed dioritic rock that intrudes the Kawabulake group yielded a TIMS U-Pb age of 1141 ± 60 Ma (four of nine grains analysed; Xiu et al. 2002), whereas a granitic gneiss yielded LA-ICP-MS U-Pb ages of 942.1 ± 7.2 and 941.9 ± 4.9 Ma (Peng et al. 2012), consistent with a Mesoproterozoic age for the Kawabulake group. Rocks of the Kawabulake group have been locally metamorphosed to greenschist facies during the Palaeozoic Central Tianshan Orogeny.

Ore geology and pyrite paragenesis

Sulphide mineralization at Caixiashan occurs principally within the recrystallized dolomite and calcite of the Kawabulake group (Cao et al. 2013). The mineralization is syn-tectonic and focused along normal faults. Some of the ore bodies have been overprinted by local tremolite alteration caused by contact metamorphism associated with Carboniferous dioritic dikes indicating that the mineralization is pre ~350 Ma (Fig. 1c).

Based on the mineral assemblages and crosscutting relationships, the mineral paragenesis is divided into four stages (Li et al. 2015b): the syn-sedimentary stage I, the sulphide-carbonate stage II, the magmatic-reworking stage III and the supergene stage IV (Fig. 2). Stage I is characterised by massive pyrite (Py1) that co-precipitated with anhedral fine-grained calcite and dolomite, and is replaced by sphalerite of stage II (Fig. 2a). The Py1 is characterised by a colloform/framboidal texture (Figs. 2b, c), consistent with a sedimentary origin and is interpreted to have precipitated during sedimentation of the Kawabulake group.

Stage II is the main mineralization stage and can be subdivided into three sub-stages: the replacement pyrite alteration (II-1), the sphalerite-carbonate (II-2) and the galena-pyrite-carbonate (II-3) sub-stages. Sub-stage II-1 is characterised by layered pyrite (Py2) that occurs with recrystallized medium- to coarse-grained calcite and dolomite that can be distinguished from the fine-grained equivalents in stage I, indicating a later generation than Py1 (Fig. 2d). Py2 is also partially replaced by sphalerite and galena (Fig. 2e). Sub-stage II-2 is dominated by massive sphalerite enclosing some discrete layers of Py2 (Fig. 2f). Fine-grained pyrrhotite that displays exsolution textures was likely formed from the same fluid as the massive sphalerite, suggesting they were precipitated at the same time (Fig. 2g; Hutchison and Scott 1981). The galena veins of sub-stage II-3 cut the massive sphalerite (Fig. 2h) and commonly coexist with euhedral pyrite (Py3; Fig. 2i).

Stage III is characterised by post-mineralization tremolite overprinting sphalerite and calcite/dolomite (Fig. 2j), and by locally crosscutting quartz veins (Fig. 2k). Stage IV at Caixiashan is characterised by jarosite (Fig. 2l), which represents oxidation that is well developed along the fractures and is found down to a depth of about 17 m.

Methods

Based on the mineral paragenesis, the selected drill core samples (ZK1603, 13ZKI and 13ZKIV series) were cut in half; one side of the core was polished to identify suitable areas to sample that contained pyrite from only one stage. Individual areas were then sampled using a dental drill in order to avoid

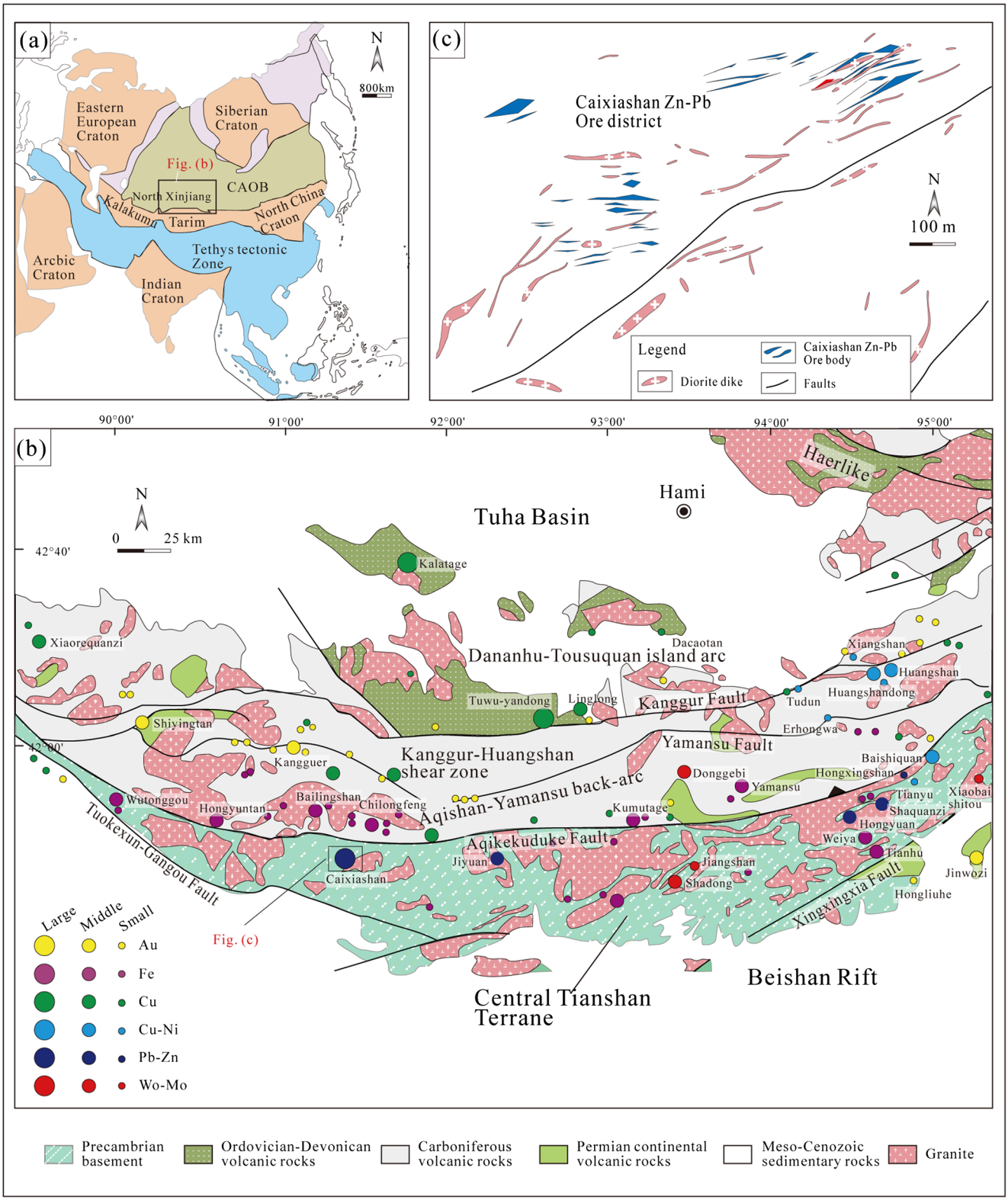

Fig. 1 Simplified geological map of Eastern Tianshan and Caixiashan Zn-Pb deposit. **a** Location of the Central Asian Orogenic Belt (CAOB) and the Tarim basin. **b** Location and major tectonic units of the Eastern Tianshan. Modified after (Deng et al. 2014). **c** Distribution of the ore bodies and dioritic dikes in the Caixiashan Zn-Pb ore district

contamination from other pyrite stages. Any vein material, areas of replacement zones, or weathering affects were avoided. Samples were rinsed with Milli-Q deionised water in an ultrasonic bath for at least 20 min. The pyrite grains were

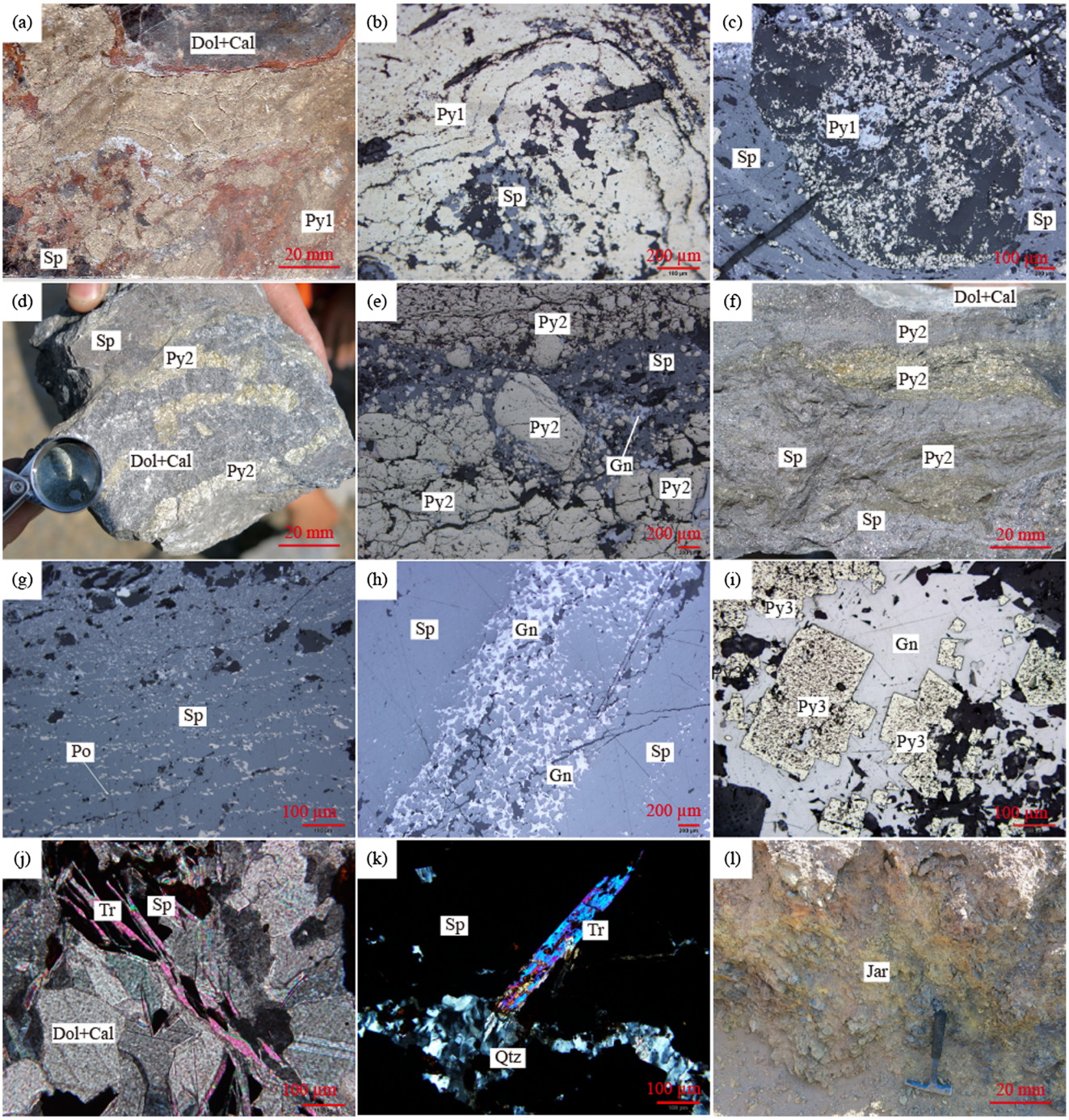

Fig. 2 Sample photographs and reflected light photomicrographs of pyrite from Caixiashan. **a** Massive pyrite (Py1) locally replaced by sphalerite. **b** Py1 showing colloform texture and replacement of the core by sphalerite. **c** Py1 showing framboidal texture. **d** Layered pyrite (Py2) coexisting with dolomite and calcite. **e** Py2 replaced by sphalerite; note that the sphalerite is cut by galena. **f** Massive sphalerite encloses discrete layers of Py2. **g** Fine-grained pyrrhotite showing exsolution texture in massive sphalerite. **h** Massive sphalerite replaced by vein galena. **i** Euhedral pyrite (Py3) coexisting with galena. **j** Tremolite overprinting sphalerite, dolomite and calcite. **k** Quartz vein crosscutting the sphalerite and euhedral tremolite outgrowth from quartz vein. **l** Outcrop of jarosite. *Py* pyrite, *Sp* sphalerite, *Po* pyrrhotite, *Gn* galena, *Dol* dolomite, *Cal* calcite, *Jar* jarosite

crushed in an agate mortar then passed through a 60# sieve (<350 μm). Sulphide samples smaller than 350 μm were separated from tremolite and jarosite using Lithium Metatungstate (LMT) Heavy Liquid (MT Liquid, llc, United States). The sulphide separates were then washed three times in an ultrasonic acetone bath.

Re-Os dating of pyrite was undertaken at the State Key Laboratory of Isotope Geochemistry, Guangzhou Institute of

Geochemistry, Chinese Academy of Sciences, utilising an analytical method based on Li et al. (2014b). Approximately 0.8 g of powder was weighed and placed in Carius tubes. Appropriate amounts of the individual ^{185}Re and ^{190}Os spike solutions were accurately weighed and carefully added to each sample tube. The tubes were chilled in a bath containing a freezing mixture of liquid N_2 and ethanol, and 2.5 ml of concentrated HCl and 7.5 ml of concentrated HNO_3 were successively added. The Carius tubes were carefully sealed and heated in an oven at 230 °C for 24 h. After decomposition, the glass tubes were again chilled in a bath of liquid N_2 and ethanol before opening. After thawing, the contents were poured into 20-ml centrifuge tubes to allow precipitation of residual solids. The supernatant solutions were transferred into 30-ml PFA (Perfluoroalkoxy) vials and subjected to Os solvent extraction by CCl_4 followed by back-extraction into concentrated HBr. The detailed solvent extraction procedure and conditions have been described in prior studies (Cohen and Waters 1996). The extracted Os fraction was further purified by micro distillation prior to N-TIMS analysis (Birck et al. 1997). Osmium was loaded in HBr on 99.999 % Pt filaments (H. Cross Company, USA), and $Ba(OH)_2$ emitter solution was loaded on top of the sample to enhance ion emission. Os and Re isotopic compositions were measured in pulse-ion-counting electron multiplier mode and in static multiple Faraday collector mode, respectively. Details of the analytical procedure are described elsewhere (Walker et al. 2005).

After Os extraction, the remaining solutions were evaporated to dryness, and the residues were dissolved in 1 ml of 6 mol l^{-1} HCl. The solutions were again evaporated to dryness, and the residues were re-dissolved in 10 ml of 1 mol l^{-1} HCl on a hot plate at 120 °C. Bio-Rad Poly-Prep columns filled with 1.8-ml pre-cleaned anion exchange resin (Bio-Rad, AG1X8, 100–200 mesh) were used for the separation and purification of Re (Morgan and Walker 1989). Finally, Re mass fractions were determined by ID-ICP-MS (Thermo Elemental X2 series; Thermo Fisher Scientific, Waltham, MA, USA). Peak hopping with short dwell times of 30 ms (measurement time on peak) was undertaken to provide quasi-simultaneous measurement. The details of the ICP-MS analyses are described elsewhere (Li et al. 2014a). Total procedural blanks (TPB) for this technique were 0.32 ± 0.14 pg with the $^{187}Os/^{188}Os$ ratio of 0.284 ± 0.049 (n = 6, 1 s) on average for Os and between 6 and 8 pg for Re. Blank contributions were typically (with the highest blank contribution in brackets) <1 % (2 %) for Re and <2 % (5 %) for Os, respectively.

Repeated analyses of the Os standard solution (Merck Chemical AA standard solution) yielded a mean $^{187}Os/^{188}Os$ value of 0.1202 ± 3 (2 SD, n = 12) for the period of analysis. Uncertainties were determined by the uncertainties of the blank, the ^{187}Re decay constant of 1.666×10^{-11} a^{-1} (Smoliar et al. 1996), and the ^{185}Re and ^{190}Os spike calibrations, which are reported at the 1-sigma level with the associated error correlation function rho (Ludwig 1980). The ages were plotted using Isoplot v 3.0 (Ludwig 2003).

Re-Os results

Total Re and Os abundances in Py1 range from 5.09–19.57 and 0.229–0.405 ppb, respectively, with $^{187}Re/^{188}Os$ ratios ranging from 89.1–464 and $^{187}Os/^{188}Os$ from 1.425–7.729 (Table 1). The samples show a positive correlation (R^2 = 0.997, 0.994 and 0.997, respectively; R^2 = coefficient of determination) on the $^{187}Re/^{188}Os$ vs. $^{187}Os/^{188}Os$ diagram (Fig. 3a). Py1 yielded a well-defined individual model 3 Re-Os isochron age (2σ uncertainty) of 1019 ± 70 Ma (MSWD = 3.5, initial $^{187}Os/^{188}Os$ ratio [I_{Os}] = −0.11 ± 0.33; Fig. 3a).

Re and Os abundances in Py2 range from 5.05–13.47 and 0.146–0.575 ppb, with $^{187}Re/^{188}Os$ ratios of 72.8–343.4 and $^{187}Os/^{188}Os$ ratios of 1.293–5.057 (Table 1). Py2 yielded a well-defined individual model 3 Re-Os isochron age (2σ uncertainty) of 859 ± 79 Ma (MSWD = 6.7, initial $^{187}Os/^{188}Os$ ratio [I_{Os}] = 0.19 ± 0.25; Fig. 3b). The Py3 separates contain Re and Os concentrations of 3.47–29.29 and 0.612–2.453 ppb, respectively with $^{187}Re/^{188}Os$ ratios of 17.8–262 and $^{187}Os/^{188}Os$ of 0.402–3.832 (Table 1). Py3 yielded a well-defined individual model 3 Re-Os isochron age of 837 ± 39 Ma (MSWD = 6.5, initial $^{187}Os/^{188}Os$ ratio [I_{Os}] = 0.16 ± 0.09; Fig. 3c).

Implications of pyrite Re-Os isochron ages

The Re-Os isochron age (1019 ± 70 Ma; MSWD = 3.5; 2σ uncertainty) of the syn-sedimentary pyrite (Py1) is within error of the single grain zircon TIMS U-Pb age of 1141 ± 60 Ma for a metamorphosed diorite (Xiu et al. 2002) and older than the U-Pb age of 942.1 ± 7.2 Ma (n = 12; MSWD = 0.75) and 941.9 ± 4.9 Ma (n = 12; MSWD = 1.18; 2σ uncertainty) from a granitic gneiss (Peng et al. 2012) intruded into the Kawabulake group. Thus, the current best estimate of the depositional age of the Kawabulake group is 1019 ± 70 Ma. The negative initial $^{187}Os/^{188}Os$ ratio of −0.11 ± 0.33 has a large uncertainty. Similar negative initial $^{187}Os/^{188}Os$ ratios have been reported for the initial $^{187}Os/^{188}Os$ ratios calculated for pyrite from the Polaris MVT deposit in Canada, which were interpreted as being the result of post formation disturbances (Selby and Creaser 2003; Selby et al. 2005), and a similar process may have occurred at Caixiashan.

The petrography and crosscutting relationships of Py2 and Py3 indicate that the main Zn mineralization formed after the Py2 but before the Py3 stage, whereas the Pb (stage II-3) is broadly synchronous with Py3; therefore, ages of Py2 and Py3

Table 1 Re-Os Isotope data for pyrite in the Caixiashan Zn-Pb deposit, Xinjiang

Sample No.	Stage	Sample wt (g)	Total Re (ppb)	2σ	Total Os (ppb)	2σ	^{192}Os (ppt)	2σ	^{187}Re/^{188}Os	2σ	^{187}Os/^{188}Os	2σ	Rho[a]
IZK1603-1	Py1	0.8025	19.57	0.20	0.405	0.001	82.49	0.25	464.0	4.9	7.729	0.021	0.801
IZK1603-2		0.8035	6.21	0.06	0.229	0.003	69.51	0.79	175.5	2.7	2.762	0.029	0.746
IZK1603-3		0.8159	5.09	0.05	0.322	0.003	112.42	1.11	89.1	1.2	1.425	0.012	0.902
IZK1603-5		0.7976	11.25	0.09	0.302	0.003	74.30	0.78	296.7	3.9	5.142	0.050	0.869
IZK1603-6		0.8148	11.46	0.04	0.310	0.002	77.72	0.59	289.0	2.4	4.922	0.040	0.730
IZK1603-9		0.8074	12.04	0.08	0.301	0.003	72.37	0.64	325.9	3.6	5.442	0.047	0.947
13ZKI-T1	Py2	0.8628	13.47	0.14	0.345	0.003	88.46	0.79	298.4	4.0	4.618	0.040	0.926
13ZKI-T2		0.8600	7.55	0.03	0.575	0.010	204.09	3.50	72.8	1.3	1.293	0.007	0.725
13ZKI-T3		0.8675	5.05	0.05	0.251	0.001	81.89	0.36	121.2	1.3	2.050	0.010	0.995
13ZKI-T5		0.8393	6.33	0.14	0.186	0.003	52.41	0.72	236.8	6.2	3.558	0.047	0.983
13ZKI-T6		0.8639	6.33	0.14	0.146	0.001	42.99	0.27	343.4	7.9	5.057	0.030	0.837
13ZKI-T7		0.8661	6.75	0.13	0.293	0.002	94.90	0.57	139.7	2.7	2.128	0.015	0.885
13ZKI-T8		0.8639	6.22	0.15	0.273	0.003	89.47	1.01	136.7	3.6	2.006	0.021	0.828
13ZKIV-T1	Py3	0.8648	29.29	0.18	0.799	0.003	219.31	0.89	262.0	1.9	3.832	0.014	0.776
13ZKIV-T2		0.8682	20.32	0.16	0.630	0.003	180.38	0.84	221.1	2.1	3.374	0.017	0.815
13ZKIV-T3		0.8592	4.73	0.10	0.861	0.021	334.88	8.12	27.8	0.9	0.532	0.008	0.996
13ZKIV-T4		0.8663	19.40	0.40	0.615	0.002	184.19	0.54	206.8	4.3	2.897	0.006	0.924
13ZKIV-T5		0.8696	4.49	0.06	0.612	0.013	233.09	5.07	37.9	1.0	0.694	0.012	0.891
13ZKIV-T6		0.8767	13.84	0.07	0.783	0.005	269.42	1.61	101.1	0.8	1.567	0.009	0.734
13ZKIV-T7		0.8685	10.96	0.05	2.453	0.053	956.06	20.56	22.6	0.5	0.512	0.005	0.925
13ZKIV-T8		0.8614	3.47	0.04	0.975	0.011	385.49	4.35	17.8	0.3	0.402	0.002	0.833

[a] Rho is the associated error correlation (Ludwig 1980)

can constrain the maximum and minimum age of the mineralization. Consequently, based on the Re-Os isochron ages for these two pyrite stages, the precipitation of Zn and Pb likely occurred at 859 ± 79 and 837 ± 39 Ma, respectively. The isochron ages of these two stages are overlapping within error but can be distinguished by their crosscutting relationships (Fig. 2h).

Post-ore diorite dikes emplaced in or around the Zn-Pb ore bodies (Fig. 1c) have yielded zircon U-Pb ages of ca. 350 Ma (Li et al. 2015a), indicating an Early Carboniferous age. Although some of the dikes show close spatial relationship to the Caixiashan ore body, the Re-Os ages of Py1, Py2 and Py3 preclude any genetic relationship between mineralization and diorite dikes.

Osmium and pyrite sources

The Caixiashan Zn-Pb deposit shows petrographic, fluid geochemistry (Li et al. 2015b) and mineralization styles similar to the Pb-Zn deposits found in the Irish ore field (Wilkinson 2010; Wilkinson and Hitzman 2014). The I_{Os} values for pyrite isochrons can be used to distinguish between seawater, hydrothermal and mantle sources (Ravizza and Turekian 1989; Cohen et al. 1999; Selby and Creaser 2003; Rooney et al. 2011; Sperling et al. 2014). The I_{Os} values of Py2 and Py3 from the Neoproterozoic Caixiashan Zn-Pb deposit (I_{Os} = 0.19 and 0.16, respectively) are much lower than Neoproterozoic sea water values (~0.8–1.0; Rooney et al. 2011) but are similar to Mesoproterozoic seawater I_{Os} compositions of 0.29–0.33 (Kendall et al. 2009; Rooney et al. 2010). Sedimentary rocks of the Mesoproterozoic Kawabulake group, which form the immediate basement rocks to the Caixiashan deposit, most likely record the Mesoproterozoic seawater I_{Os} composition. Therefore, one explanation is that the zinc- and lead-bearing hydrothermal fluid leached Os from the footwall Mesoproterozoic sedimentary rocks. This explanation is further supported by Pb-S-C-O isotopic compositions of the ore-forming minerals that indicate metals were sourced from sedimentary rocks in the Kawabulake group (Gao et al. 2007). However, because deposition of the host rocks occurred at least 150 Ma before ore deposit formation, the radiogenic decay would result in more radiogenic I_{Os} values than those observed in this study, and therefore, the host sedimentary rocks are not thought to have been the source for the osmium.

An alternative explanation for the relatively unradiogenic I_{Os} values is derivation from a source with mantle characteristics (I_{Os} = 0.13; Meisel et al. 2001) with some mixing with upper continental crustal material (I_{Os} > 0.13; Peucker-Ehrenbrink and

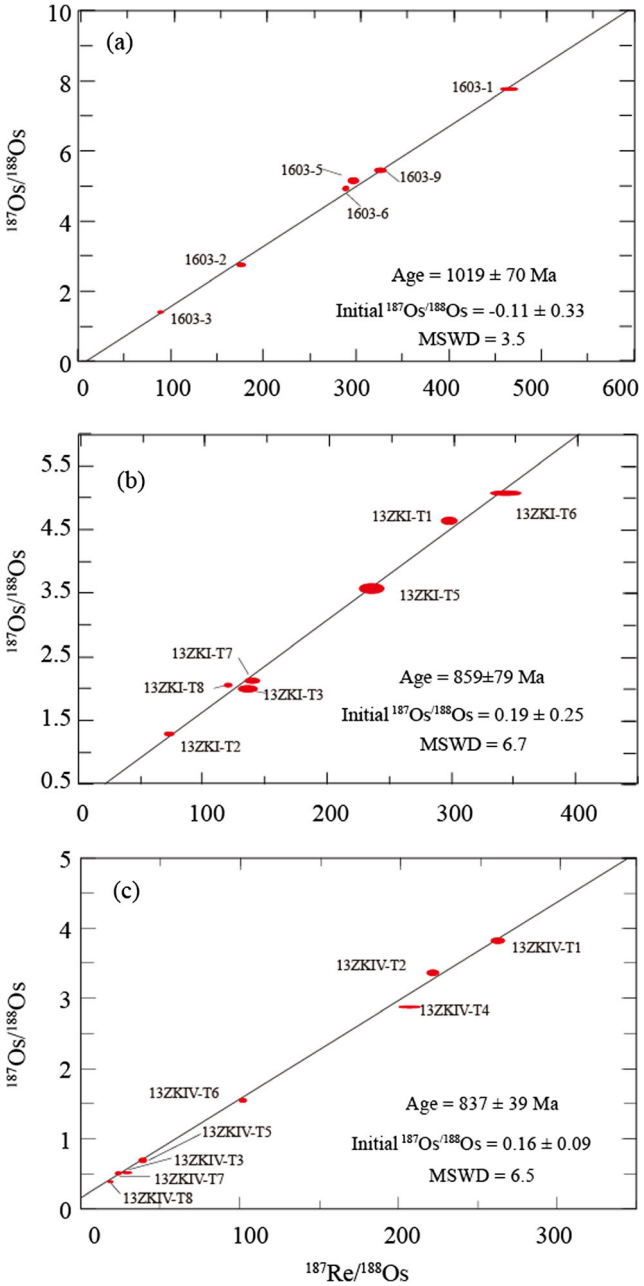

Fig. 3 $^{187}Re/^{188}Os$ vs. $^{187}Os/^{188}Os$ plots for pyrite separates from the Caixiashan Zn-Pb deposit. *Plots a*, *b* and *c* represent pyrite separates from the three main stages of mineralization. Sample numbers are keyed to Table 1

Jahn 2001). However, as direct derivation from the mantle is unlikely, it is possible that mantle derived rocks within the crust may have acted as a source for the unradiogenic I_{Os}. High ore-forming temperatures (ca. 270 °C; Li et al. 2015b) are consistent with deep fluid sources. Wilkinson and Hitzman (2014) advocate for magmatic heat, derived from the underplating of mid-crustal sills, as a driver for the regional flow associated with Irish-type deposits. This model explains the unusual high fluid temperatures documented in the Irish orefield and the low radiogenic initial Os contents of both the Lisheen (0.253 ± 0.045) and Silvermine (0.453 ± 0.006) deposits (Hnatyshin et al. 2015) and may account for the unradiogenic values found in this study. The existence of 830–740-Ma magmatic events in the northern Tarim block (Xu et al. 2005; Zhan et al. 2007; Zhu et al. 2008) may have provided a possible heat source to generate these hydrothermal fluids. Slack et al. (2015) in a study of the black shale-hosted Red Dog Zn-Pb-Ag deposit showed that the unradiogenic I_{Os} in pyrite veins could have been derived from hydrothermal fluids that leached mafic and ultramafic rocks that occurred at depth under the deposit. It is possible that broadly coeval rift-related magmas may have acted as a source for unradiogenic Os in the Caixiashan deposit through leaching by ore fluids.

Implications for tectonic setting and metallogenesis

The Mesoproterozoic to middle Neoproterozoic tectonic framework of the northern Tarim basin has been interpreted to be either a continental rift or a passive continental margin (Zhu et al. 2011). Rocks of the Kawabulake group are located in the northeastern part of the Tarim basin and are believed to reflect rifting of a passive continental margin and concurrent deposition of sediment on a subsiding continental slope (Dong 2005). The Kawabulake group is considered to have formed during the Mesoproterozoic. The stratigraphic position of the Kawabulake group sedimentary rocks indicates that they were deposited no later than the Mesoproterozoic Xingxingxia group, which has been dated based on the occurrence of stromatolites (e.g., *Conophyton cylindrical*; Dong 2005) and intrusive relationships with meta-diorite that yielded a U-Pb age of 1141 ± 60 Ma (Xiu et al. 2002) and granitic gneiss with ages of 942.1 ± 7.2 and 941.9 ± 4.9 Ma (Peng et al. 2012). The syn-sedimentary pyrite (Py1) from the Kawabulake group yielded an isochron age of 1019 ± 70 Ma indicating it was deposited during the Grenville orogeny (ca. 1300–900 Ma; Song et al. 2012).

The Eastern Tianshan lies in a key position in the Central Asian Orogenic Belt. Several Palaeozoic metallogenic epochs have been identified in the Eastern Tianshan area (Zhang et al. 2008; Han et al. 2014), but there are no reports of Precambrian mineralization, in part, because most of the sedimentary-hosted deposits in this area lack accurate ages for the time of deposition and because the Palaeozoic magmatism and regional metamorphism have reworked the ore bodies and the host rocks. Due to these complexities, the genesis of these deposits has long been a matter of debate. For example, the hydrothermal fluids at Caixiashan have been proposed to be either some form of magmatic fluid (Cao et al. 2013) or sedimentary brines (Peng et al. 2007). The new pyrite ages that bracket the mineralization preclude derivation from Palaeozoic magmatic hydrothermal fluids, and

suggest the presence of a newly identified Neoproterozoic metallogenic event in the Eastern Tianshan, particularly within the Mesoproterozoic Kawabulake group and that the ore-forming fluids have both magmatic and sedimentary source components.

A Neoproterozoic continental rift setting for the Kawabulake group has been suggested based on multiple 830–740-Ma magmatic events in the northern Tarim block related to the breakup of Rodinia (Chen et al. 2004; Huang et al. 2005; Xu et al. 2005; Zhan et al. 2007; Zhang et al. 2007; Zhu et al. 2008). The ore-forming process at Caixiashan likely occurred in an extensional environment, in which oxidised sulphate-containing fluids descended through the permeable and oxidised clastic aquifer or fractured basement and leached the metals from the sediment and from inferred mafic to ultramafic source rocks within the basement stratigraphy, forming an oxidised metalliferous fluid enriched in Zn and Pb, that mixed with likely sources of reduced sulphur including one formed by sulphate reduction facilitated by organic matter or bacteria in the organic-rich sediments (CH_4) or reduced basin fluids (Leach et al. 2010). Minor magmatic heat produced by magmatic events from 830–740 Ma may have acted as a driver for the regional fluid flow with the same magmas possibly providing a source for the unradiogenic osmium.

Conclusions

This study provides geochronological evidence for both syn-sedimentary pyrite and pyrite associated with mineralization, which constrains the age of the mineralization process at Caixiashan. The Kawabulake group rocks host the Caixiashan Zn-Pb deposit and were deposited in the northern Tarim at 1019 ± 70 Ma with the main mineralization stage of Caixiashan occurring between 859 ± 79 and 837 ± 39 Ma. The new Re-Os ages are interpreted to represent a newly identified mineralization epoch in the Eastern Tianshan of the Central Asia Orogenic Belt. The low initial Os ratios for pyrite from the Caixiashan deposit are consistent with derivation from hydrothermal fluids that leached Os from mafic to ultramafic rocks that retained a mantle Os signature as well as from the sedimentary host rocks.

Acknowledgments This study was financial supported by the Chinese National Basic Research 973-Program (2014CB440802), the Geological Survey of China (Project 1212011140056), China Scholarship Council Fund (201404910423) and the NSFC (Nos. 41072062 and 41203029). Drs. Lu Yin and Peipei Zhao are thanked for their support in the Re-Os experiment. The Editor Georges Beaudoin, Associate Editor Karen Kelley and Dr. David Selby are thanked for constructive reviews that greatly improved the quality of this paper. This is contribution No. IS-2123 from GIGCAS.

References

Allen MB, Natal'in BA (1995) Junggar, Turfan and Alakol basins as Late Permian to? Early Triassic extensional structures in a sinistral shear zone in the Altaid orogenic collage, Central Asia. J Geol Soc London 152:327–338

Birck JL, Barman MR, Capmas F (1997) Re-Os isotopic measurements at the femtomole level in natural samples. Geostand Newsl 21:19–27

Cao XF, Lv XB, Zhang P et al (2013) Stable isotope geochemistry and ore genesis of Caixiashan Pb-Zn deposit at eastern Middle Tianshan, Xinjiang. J Cent South Univ (Sci Technol) 44:662–672

Chen Y, Xu B, Zhan S, Li Y (2004) First mid-Neoproterozoic paleomagnetic results from the Tarim Basin (NW China) and their geodynamic implications. Precambrian Res 133:271–281

Cohen AS, Waters FG (1996) Separation of osmium from geological materials by solvent extraction for analysis by thermal ionisation mass spectrometry. Anal Chim Acta 332:269–275

Cohen AS, Coe AL, Bartlett JM, Hawkesworth CJ (1999) Precise Re–Os ages of organic-rich mudrocks and the Os isotope composition of Jurassic seawater. Earth Planet Sci Lett 167:159–173

Deng X, Wang J, Wang Y, et al. (2014) Geological characteristics of the Hongshi Cu-Au deposit, eastern Tianshan, Xinjiang and discussion of the deposit genesis. Miner Explor 159–168

Dong L (2005) The split and rearrange of origin Kawabulake Group of Eastern Tianshan in Xinjiang. Xinjiang Geol 23:19–22

Gao JG, Peng MX, Liang T et al (2007) Research on geology and isotopic geochemistry of Caixiashan Pb-Zn deposit in Xinjiang. J Earth Sci Environ 29:137–140

Han C, Xiao W, Zhao G et al (2014) Late Paleozoic metallogenesis and evolution of the East Tianshan Orogenic Belt (NW China, Central Asia Orogenic Belt). Geol Ore Depos 56:493–512

Hnatyshin D, Creaser RA, Wilkinson JJ, Gleeson SA (2015) Re-Os dating of pyrite confirms an early diagenetic onset and extended duration of mineralization in the Irish Zn-Pb ore field. Geology 43:143–146

Huang B, Xu B, Zhang C et al (2005) Paleomagnetism of the Baiyisi volcanic rocks (ca. 740Ma) of Tarim, Northwest China: a continental fragment of Neoproterozoic Western Australia? Precambrian Res 142:83–92

Hutchison MN, Scott SD (1981) Sphalerite geobarometry in the Cu-Fe-Zn-S system. Econ Geol 76:143–153

Kendall B, Creaser RA, Gordon GW, Anbar AD (2009) Re-Os and Mo isotope systematics of black shales from the Middle Proterozoic Velkerri and Wollogorang formations, McArthur Basin, northern Australia. Geochim Cosmochim Acta 73:2534–2558

Lawley CJM, Selby D (2012) Re-Os geochronology of quartz-enclosed ultrafine molybdenite: implications for ore geochronology. Econ Geol 107:1499–1505

Lawley C, Selby D, Imber J (2013) Re-Os molybdenite, pyrite, and chalcopyrite geochronology, Lupa goldfield, southwestern Tanzania: tracing metallogenic time scales at midcrustal shear zones hosting orogenic Au deposits. Econ Geol 108:1591–1613

Leach DL, Bradley DC, Huston D et al (2010) Sediment-hosted lead-zinc deposits in earth history. Econ Geol 105:593–625

Li J, Jiang XY, Xu JF et al (2014a) Determination of platinum-group elements and Re-Os isotopes using ID-ICP-MS and N-TIMS from a single digestion after two-stage column separation. Geostand Geoanal Res 38:37–50

Li J, Zhao PP, Liu J et al (2014b) Reassessment of hydrofluoric acid desilicification in the carius tube digestion technique for Re-Os isotopic determination in geological samples. Geostand Geoanal Res. doi:10.1111/j.1751-908X.2014.00299.x

Li DF, Zhang L, Chen HY et al (2015a) Geochronology and geochemistry of the high Mg dioritic dikes in Eastern Tianshan, NW China:

geochemical features, petrogenesis and tectonic implications. J Asian Earth Sci 115:442–454

Li DF, Chen HY, Zhang L et al (2015b) Ore geology and fluid evolution of the giant Caixiashan carbonate-hosted Zn–Pb deposit in the Eastern Tianshan, NW China. Ore Geol Rev 72:355–372

Ludwig KR (1980) Calculation of uncertainties of U-Pb isotope data. Earth Planet Sci Lett 46:212–220

Ludwig KR (2003) User's manual for Isoplot 3.00: a geochronological toolkit for Microsoft Excel. Berkeley Geochronology Centre Special Publication No. 4

Meisel T, Walker RJ, Irving AJ, Lorand J-P (2001) Osmium isotopic compositions of mantle xenoliths: a global perspective. Geochim Cosmochim Acta 65:1311–1323

Morelli RM, Creaser RA, Selby D et al (2004) Re-Os sulfide geochronology of the red dog sediment-hosted Zn-Pb-Ag deposit, Brooks Range, Alaska. Econ Geol 99:1569–1576

Morgan JW, Walker RJ (1989) Isotopic determinations of rhenium and osmium in meteorites by using fusion, distillation and ion-exchange separations. Anal Chim Acta 222:291–300

Peng MX, Wang JL, Yu WY et al (2007) Geological characteristics features and building about respexting-model of the Caixiashan lead-zinc deposit in the Shanshan, Xinjiang. Xinjiang Geol 24:405–411

Peng MX, Sang SJ, Zhu C et al (2008) Forming analysis of the Caixiashan lead-zinc deposit Xinjiang and comparison with the MVT depost. Xinjiang Geol 25:373–378

Peng MX, Zhong CG, Zuo QH et al (2012) The formation age and their geological significance of gneissose granites neighbouring Kawabulake area in East Tianshan Mountain. Xinjiang Geol 30: 12–18

Peucker-Ehrenbrink B, Jahn B (2001) Rhenium-osmium isotope systematics and platinum group element concentrations: loess and the upper continental crust. Geochem Geophys Geosyst 2:1061. doi:10.1029/2001GC000172

Pirajno F, Mao J, Zhang Z et al (2008) The association of mafic–ultramafic intrusions and A-type magmatism in the Tian Shan and Altay orogens, NW China: implications for geodynamic evolution and potential for the discovery of new ore deposits. J Asian Earth Sci 32:165–183

Ravizza G, Turekian KK (1989) Application of the ^{187}Re-^{187}Os system to black shale geochronometry. Geochim Cosmochim Acta 53:3257–3262

Rooney AD, Selby D, Houzay JP, Renne PR (2010) Re-Os geochronology of a Mesoproterozoic sedimentary succession, Taoudeni basin, Mauritania: implications for basin-wide correlations and Re-Os organic-rich sediments systematics. Earth Planet Sci Lett 289:486–496

Rooney AD, Chew DM, Selby D (2011) Re-Os geochronology of the Neoproterozoic-Cambrian Dalradian Supergroup of Scotland and Ireland: implications for Neoproterozoic stratigraphy, glaciations and Re-Os systematics. Precambrian Res 185:202–214

Selby D, Creaser RA (2003) Re-Os geochronology of organic rich sediments: an evaluation of organic matter analysis methods. Chem Geol 200:225–240

Selby D, Creaser RA, Dewing K, Fowler M (2005) Evaluation of bitumen as a ^{187}Re–^{187}Os geochronometer for hydrocarbon maturation and migration: a test case from the Polaris MVT deposit, Canada. Earth Planet Sci Lett 235:1–15

Selby D, Kelley KD, Hitzman MW, Zieg J (2009) Re-Os sulfide (bornite, chalcopyrite, and pyrite) systematics of the carbonate-hosted copper deposits at Ruby Creek, southern Brooks Range, Alaska. Econ Geol 104:437–444

Slack JF, Selby D, Dumoulin JA (2015) Hydrothermal, biogenic, and seawater components in metalliferous black shales of the Brooks Range, Alaska: synsedimentary metal enrichment in a carbonate ramp setting. Soc Econ Geol 110:653–675

Smoliar MI, Walker RJ, Morgan JW (1996) Re-Os ages of group IIA, IIIA, IVA, and IVB iron meteorites. Science 271:1099–1102

Song S, Su L, Li X et al (2012) Grenville-age orogenesis in the Qaidam-Qilian block: the link between South China and Tarim. Precambrian Res 220:9–22

Sperling EA, Rooney AD, Hays L et al (2014) Redox heterogeneity of subsurface waters in the Mesoproterozoic ocean. Geobiology 12: 373–386

Stein HJ, Sundblad K, Markey RJ et al (1998) Re-Os ages for Archean molybdenite and pyrite, Kuittila-Kivisuo, Finland and Proterozoic molybdenite, Kabeliai, Lithuania: testing the chronometer in a metamorphic and metasomatic setting. Miner Depos 33:329–345

Stein HJ, Morgan JW, Scherstén A (2000) Re-Os dating of low-level highly radiogenic (LLHR) sulfides: the Harnäs gold deposit, southwest Sweden, records continental-scale tectonic events. Econ Geol 95:1657–1671

Walker RJ, Brandon AD, Bird JM et al (2005) ^{187}Os–^{186}Os systematics of Os–Ir–Ru alloy grains from southwestern Oregon. Earth Planet Sci Lett 230:211–226

Wilkinson JJ (2010) A review of fluid inclusion constraints on mineralization in the Irish ore field and implications for the genesis of sediment-hosted Zn-Pb deposits. Econ Geol 105:417–442

Wilkinson JJ, Hitzman MW (2014) The Irish Zn-Pb orofield: the view from 2014. In: Archibald SM, Piercey SJ (eds) Current perspectives in zinc deposits. Irish Association of Economic Geology, Dublin, pp 59–73

Xiu QY, Fei YH, Quan L (2002) A single zircon U-Pb age for the granodiorite of Kawabulake complex, Xinjiang, China. Xinjiang Geol 20: 335–337

Xu B, Jian P, Zheng H et al (2005) U–Pb zircon geochronology and geochemistry of Neoproterozoic volcanic rocks in the Tarim Block of northwest China: implications for the breakup of Rodinia supercontinent and Neoproterozoic glaciations. Precambrian Res 136: 107–123

Zhan S, Chen Y, Xu B et al (2007) Late Neoproterozoic paleomagnetic results from the Sugetbrak Formation of the Aksu area, Tarim basin (NW China) and their implications to paleogeographic reconstructions and the snowball Earth hypothesis. Precambrian Res 154:143–158

Zhang C-L, Yu H-F, Haimin Y (2007) Discussions on the Neoproterozoic diorites in central Tarim basin: a comment on "Geochronology and geochemistry of deep-drill-core samples from the basement of the central Tarim basin" by Guo et al. (Journal of Asia Earth Sciences, 2005, vol. 25, 45–56). J Asian Earth Sci 29:177–180

Zhang L, Qin K, Xiao W (2008) Multiple mineralization events in the eastern Tianshan district, NW China: isotopic geochronology and geological significance. J Asian Earth Sci 32:236–246

Zhu WB, Zhang ZY, Shu LS et al (2008) SHRIMP U–Pb zircon geochronology of Neoproterozoic Korla mafic dykes in the northern Tarim Block, NW China: implications for the long-lasting breakup process of Rodinia. J Geol Soc London 165:887–890

Zhu W, Zheng B, Shu L et al (2011) Neoproterozoic tectonic evolution of the Precambrian Aksu blueschist terrane, northwestern Tarim, China: insights from LA-ICP-MS zircon U-Pb ages and geochemical data. Precambrian Res 185:215–230